nature communications

Article

https://doi.org/10.1038/s41467-025-60572-0

Chiral substrate-induced chiral covalent organic framework membranes for enantioselective separation of macromolecular drug

Received: 31 December 2024

Accepted: 28 May 2025

Published online: 05 June 2025

Check for updates

Xiaoyue Gao[1] & Teng Ben[1,2,3]

Chiral drugs are essential in modern medicine, but separating their enantiomers is challenging due to their similar physicochemical properties. However, traditional methods are often costly and inefficient. Here we show that chiral covalent organic framework (CCOF-300) membranes, induced by chiral dopants (L-(+)-/D-(−)-tartaric acid), can achieve high enantioselectivity in separating chiral drugs. Specifically, CCOF-300 membrane achieved 100% enantiomeric excess in separating racemic N-Fmoc-N′-[1-(4,4-Dimethyl−2,6-dioxocyclohexylidene)ethyl]-lysine (Fmoc-Lys(Dde)-OH). We found that size matching and differences in diffusion rates between enantiomers are key factors in chiral separation. Additionally, there were no significant differences in the binding energy between ibuprofen (IBU), Fmoc-Lys(Dde)-OH, and CCOF-300, indicating that binding energy is not the dominant factor in chiral separation. This study proposes a cost-effective and scalable method for chiral drug separation, highlighting the potential of chiral induction strategy in improving chiral separation technology in the pharmaceutical industry.

The global pharmaceutical market is increasingly dominated by chiral drugs, projected to exceed USD 140 billion by 2025[1–4]. These drugs, comprising enantiomerically pure compounds, are crucial in treating a broad spectrum of conditions due to the unique and often superior therapeutic properties exhibited by individual enantiomers[5–17]. However, separating enantiomers from their racemic mixtures poses a significant challenge in pharmaceutical manufacturing[18,19]. The similar physicochemical properties of enantiomers hinder traditional separation techniques, leading to high costs and limited efficiency[20,21]. Although widely used, current methods for chiral separation, such as chiral chromatography[22–26], diastereomeric crystallization[27,28], and asymmetric synthesis[29], often lack scalability and cost-effectiveness[30–33] (Supplementary Table 1). The demand for innovative and more efficient separation techniques is urgent[34].

In recent years, chiral porous materials, such as chiral metal-organic frameworks (MOFs)[35–45] and chiral covalent organic frameworks (COFs)[46–51] have become prominent for chiral drug separation. These materials provide a unique combination of high surface area, adjustable porosity, and the integration of chiral functionalities, making them excellent for selective enantiomeric separation. However, the synthesis of these materials is often constrained by the high cost of chiral building blocks, which limits their wider use[52–55]. To overcome this obstacle, the chiral-induced strategy has been introduced as a cost-efficient method for producing chiral porous materials[56]. Chiral induction can be achieved through various methods to promote the formation of chiral structures in molecules or materials[57,58]. For example, Morris et al. synthesized chiral SIMOF-1 by employing 1-butyl−3-methylimidazolium L-aspartate, an ionic liquid

[1]Department of Chemistry, Jilin University, Changchun, PR China. [2]Zhejiang Engineering Laboratory for Green Syntheses and Applications of Fluorine-Containing Specialty Chemicals, Institute of Advanced Fluorine-Containing Materials, Zhejiang Normal University, Jinhua, PR China. [3]Key Laboratory of the Ministry of Education for Advanced Catalysis Materials, Institute of Physical Chemistry, Zhejiang Normal University, Jinhua, PR China.
e-mail: tengben@zjnu.edu.cn

containing chiral anions, as the reaction medium[59]. Additionally, Bu et al. demonstrated that using (−)-cinchonidine and (+)-cinchonidine as chiral catalysts enables achiral metal ions and organic ligands to develop specific chirality during self-assembly, resulting in chiral MOFs[60]. Further studies indicated that chiral catalysts can also facilitate the synthesis of chiral COFs. For instance, (S)-DTP-COF and (R)-DTP-COF were synthesized using a chiral Cu(I)-pybox catalyst, demonstrating high efficiency in catalyzing asymmetric Michael addition reactions[61].

In addition to these methods, introducing chiral dopants represents an effective approach for chiral induction. The Zaworotko group pioneered the use of enantiomers L-proline and D-proline as chiral dopants to induce asymmetric crystallization of MOF-5, resulting in enantiomeric forms of MOF-5 with axial chirality[62]. This research garnered significant attention and subsequent studies demonstrated that various chiral dopants could synthesize chiral MOFs. For instance, chiral MOFs ($[L\text{-}HAPA]_4$ $[Cd_8(OBA)_{10}]$ and $[D\text{-}HAPA]_4[Cd_8(OBA)_{10}]$) for enantioselective sensing of chiral alkamines were achieved in the presence of the enantiomerically pure chiral dopants L- or D-2-amino-1-propanol[63]. Additionally, another study used chiral pyridine derivatives to selectively induce FJI-H27(M) and FJI-H27(P)[64]. The introduction of chiral dopants has enabled the successful synthesis of various chiral MOFs and facilitated the synthesis of chiral COFs. Cui et al. used (S)- or (R)-1- phenylethylamine as chiral dopants to synthesize chiral COFs which exhibit potential applications in asymmetric catalysis and enantioselective sensing[65]. The use of chiral dopants has also been extended to other COF systems, where the incorporation of chiral amines induces chirality, facilitating the desired chiral properties and leading to tunable circularly polarized luminescence (CPL). These findings demonstrate the wide applicability of chiral dopants in the synthesis of both chiral MOFs and COFs.

Additionally, our group effectively controlled the chirality of Eu(BTC)(H_2O)·DMF MOF by using reusable chiral dopants, such as chiral amino acids, and cost-effective achiral building blocks to create a chiral MOF with P- and M-excess (CE-MOF)[66]. Moreover, CE-MOF particles were integrated into a PIM-1 matrix to fabricate a mixed matrix membrane (Eu(BTC)(H_2O)·DMF@PIM-1 MMM) that resolves chiral organic small molecules. However, the enantiomeric excess (*ee*) value for enantiomeric separation of 2-amino-1-butanol is only 9%. We found that the performance of Eu(BTC)(H_2O)·DMF@PIM-1 MMM in chiral separation was below expectations, prompting us to further explore the potential of chiral COF membranes in chiral separation.

In recent years, chiral COF membranes have emerged as promising platforms for chiral drug separation. Pioneering studies demonstrated their potential for small chiral drug (<1.5 nm), achieving notable *ee* values up to 94.2% for naproxen[67] and 100% for tryptophan[68] through strategic incorporation of chiral building blocks. However, these membranes face significant challenges when it comes to large chiral drug (>1.8 nm), with reported *ee* values typically below 20% for antibiotics and peptide derivatives[69], primarily due to framework distortion and pore size mismatch. Moreover, current fabrication strategies relying on expensive chiral monomers or complex post-synthetic modifications face scalability challenges, highlighting an urgent need for cost-effective approaches that reconcile structural precision with industrial feasibility. The use of chiral dopants to guide the formation of a chiral framework can reduce the dependence on expensive chiral building blocks. Despite its promise, the chiral-induced strategy encounters challenges, particularly in the selection of chiral dopants. Additionally, the efficiency of chiral separation necessitates further optimization, especially for large chiral drug molecules, which continue to present significant difficulties.

In this study, we present the synthesis of chiral COF-300 using a chiral induction strategy. Building on this, we propose the sergeants-and-soldiers effect strategy and have synthesized a chiral COF-300 membrane through in-situ growth. We utilized L-(+)-/D-(−)-tartaric acid as chiral dopants, which were subsequently embedded them onto the surface of polyaniline-coated aluminum oxide substrates. This process enabled the fabrication of a chirality-induced COF-300 membrane on the substrate. Circular dichroism (CD) analysis confirmed the chiral characteristics of the synthesized chiral COF-300 membranes, which demonstrated chiral separation performance. Remarkably, the membranes achieved 100% *ee* in separating racemic Fmoc-Lys-(Dde)-OH within a specific timeframe. Detailed analysis identified that diffusion factors, especially chiral matching diffusion, predominantly controlled the enantioselective separation. Meanwhile, the efficiency of chiral separation is also strongly influenced by host-guest size matching. This research not only advances our understanding of chiral membrane synthesis technology but also introduces a cost-effective method for chiral drug separation. Our findings indicate that chiral-induced strategies hold promise for enhancing chiral separation techniques and could processes in the pharmaceutical industry.

Results

To effectively separate large chiral drug, materials with suitable pore sizes are crucial. Crystalline COF-300, possessing a uniform pore size of 1.8 nm, emerges as a promising candidate for the separation of larger drug molecules. Additionally, COF-300 exhibits a dia-seven-fold interpenetrated diamond topology, where the interpenetrated structure promotes the close packing of benzene rings along the crystal's *c*-axis via π-π stacking interactions. These robust interactions ensure the reliable transmission of chiral configurational information along the pore walls during crystal growth, allowing the entire framework to acquire chirality through chiral induction.

In accordance with established methodologies in the literature[70], we modified the synthesis process of chiral COF-300 by incorporating chiral tartaric acid as both chiral dopants and an acid catalyst (see Methods section). Tetrakis(4-aminophenyl)methane (TAPM) and terephthalaldehyde (TPA) were homogeneously dispersed in a dioxane/chiral tartaric acid mixture and subjected to a reaction at 100 °C for three days (Fig. 1). The resulting insoluble solid was isolated by filtration and subsequently washed with anhydrous ethanol, 1,4-dioxane, and tetrahydrofuran. This procedure effectively removed the chiral tartaric acid and any unreacted monomers, ultimately yielding a high-purity yellow chiral COF-300 (Λ-CCOF-300/Δ-CCOF-300) powder with a yield of 78%.

We investigated the impact of chiral tartaric acid quantity on the synthesis of CCOF-300 by varying the molar ratio of carboxyl groups in chiral tartaric acid to amino groups in TAPM (1:1, 1:5, 1:10, 1:20). The results indicated that no solid product was observed at molar ratios of 1:1 and 1:20, whereas highly crystalline CCOF-300 was obtained at molar ratios of 1:5 and 1:10. Fourier transform infrared spectroscopy (FT-IR) clearly showed the disappearance of characteristic peaks from the amino groups (3390 cm^{-1}) and aldehyde groups (1690 cm^{-1}) present in the monomers (Supplementary Fig. 1). Simultaneously, a new signal at 1620 cm^{-1}, attributed to C = N bond stretching, indicated the formation of imine bonds. No evidence of the chiral dopants appeared in the FT-IR spectrum, suggesting the absence of chiral tartaric acid within the pores of CCOF-300. Supplementary Figs. 2–5 illustrate the ^1H nuclear magnetic resonance (NMR) spectrum of acid-digested COF in DMSO-d_6, which reveals the stoichiometric ratio of TPAM and TPA as 2:1. Hence, we propose the following mechanism of chiral induction (Supplementary Fig. 6): First, TAPM combines with chiral tartaric acid (chiral dopants) via hydrogen bonding to form transitional chiral building blocks. TPA then attacks these chiral building blocks, affording chirality-enriched entities. Powder X-ray diffraction (PXRD) patterns showed that the CCOF-300 resembled achiral COF-300, implying that the introduction of the chiral dopants did not alter the crystal structure (Supplementary Figs. 7, 8). Scanning Electron Microscope (SEM) images indicated that CCOF-300 powder retained a

https://doi.org/10.1038/s41467-025-60572-0

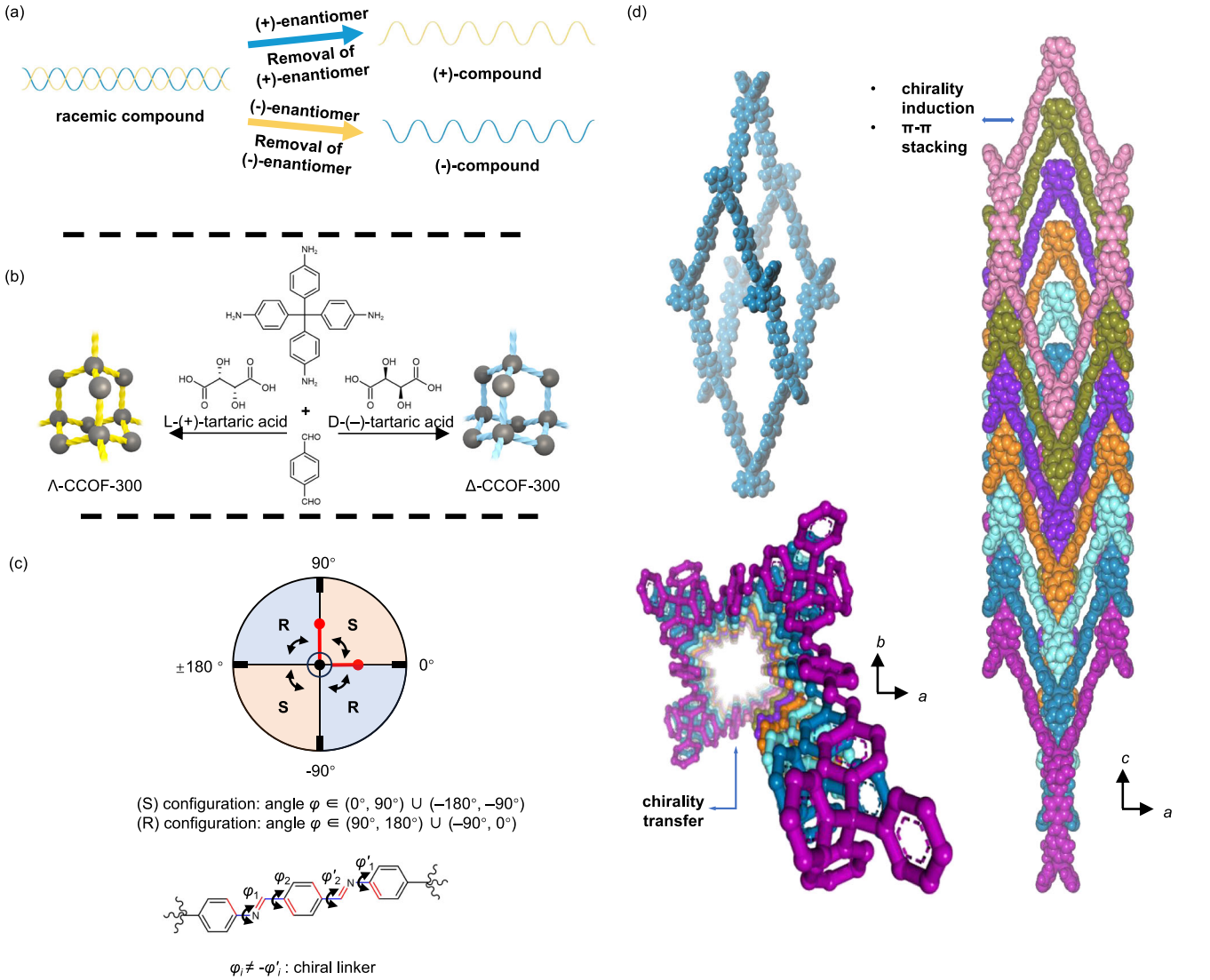

Fig. 1 | Chiral induction and transfer mechanisms in the synthesis and structural conformations of CCOF-300. a Mechanism of chiral induction. **b** Synthesis of CCOF-300. **c** Conformations of linkers in COF-300. $\varphi_i = -\varphi'_i$ corresponds to the achiral linker, while $\varphi_i \neq -\varphi'_i$ corresponds to the chiral linker[71]. **d** Chiral transfer mechanism diagram.

spindle-like morphology similar to COF-300 (Supplementary Figs. 9, 10). CD (Supplementary Fig. 11) shows that both Λ-CCOF-300 and Δ-CCOF-300 exhibit a near-mirror cotton effect in the 300 – 600 nm wavenumber range. Similarly, vibrational circular dichroism (VCD) (Supplementary Fig. 12) demonstrates that the same compounds display a near-mirror cotton effect in the wavenumber range 1300 – 900 cm^{-1}, supporting that two nearly opposite chiral diastereoisomeric COF channel have been induced and prepared in the presence of L-(+)-tartaric acid or D-(−)-tartaric acid, respectively. These results demonstrated that introducing chiral dopants could asymmetrically arrange the achiral COF-300 framework, resulting in chiral CCOF-300.

During the preparation of this manuscript, we became aware that Sun's group had employed a similar methodology (Fig. 1c)[71]. They used chiral amino acid derivatives as chiral dopants to disrupt the meso structure of COF-300 during synthesis, resulting in chiral single crystals and elucidating the precise mechanism of chiral induction. In COF-300_L-cp and COF-300_D-cp, alterations in the dihedral angles of the connecting groups (φ_1, φ'_1, φ_2, φ'_2) led to different conformational chirality. It is important to note that our study utilizes chiral tartaric acid as the chiral dopant, which results in distinct chiral signals, as confirmed by CD spectroscopy.

Based on the aforementioned experimental evidence, we further investigated the feasibility of applying this method for in-situ chirality induced chiral COF-300 membrane growth. Porous alumina sheets were selected as substrates and modified them with polyaniline via spin coating[72], followed by immersion in a 2.0 mol L^{-1} solution of L-(+)- or D-(−)-tartaric acid for secondary modification. During this process, the color of the polyaniline-coated aluminum oxide substrate changed from blue to green. This phenomenon is attributed to the protonation of the emeraldine base form of polyaniline under acidic conditions, which results in the formation of emeraldine salt, typically exhibiting a green color[73,74]. Consequently, the chiral tartaric acid can be anchored on the surface of the polyaniline layer due to charge interactions, thereby providing numerous surface chiral active bonding sites. Building on this, the preparation of the chiral COF-300 membrane involved the following steps (Fig. 2a): 36.0 mg (0.3 mmol) of TPA and 60.0 mg (0.2 mmol) of TAPM were added to a 50 mL reactor, followed by 9 mL of anhydrous 1,4-dioxane. The mixture was then sonicated to ensure complete dissolution, yielding a clear yellow solution.

https://doi.org/10.1038/s41467-025-60572-0

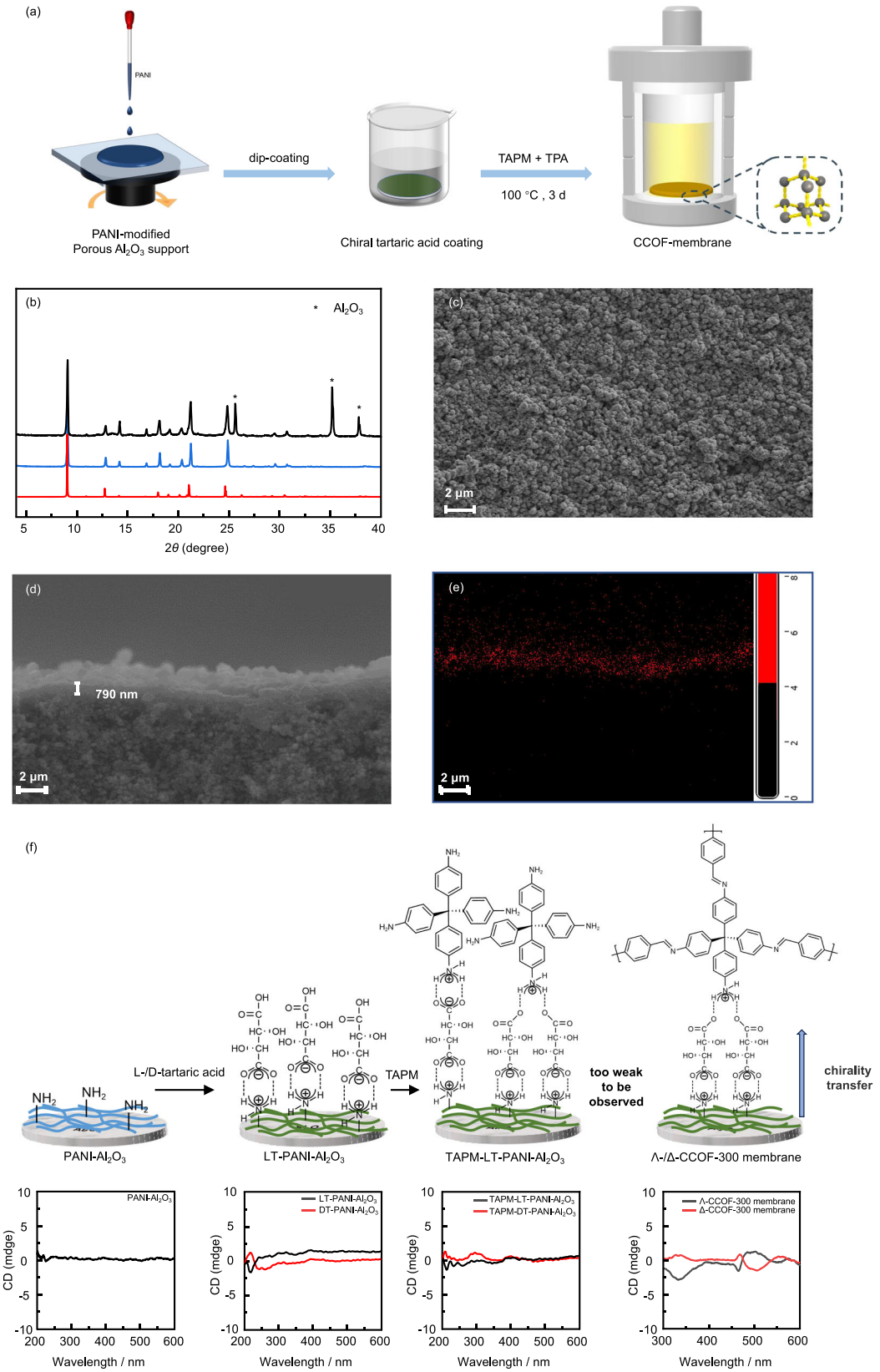

Fig. 2 | Characterization and structural analysis of the CCOF-300 membrane. **a** Synthesis of CCOF-300 membrane. **b** XRD patterns of CCOF-300 membrane (black line), COF-300 powder (blue black) and simulated data (red line). SEM images of **c** surface of the CCOF-300 membrane and **d** cross-section of the CCOF-300 membrane and **e** corresponding elemental mapping image of carbon. **f** Mechanism of chiral-induced membrane formation.

Subsequently, 0.6 mL of 3 M acetic acid aqueous solution was gradually added while stirring. It is important to note that the acetic acid catalyst does not possess chiral induction capabilities, all chiral induction factors arise from the adsorption of small-molecule chiral tartaric acid on the substrate surface. The modified substrate was then quickly placed into the reactor with the modified side facing upward, and the reactor was sealed. After 24 h of treatment at 100 °C, a continuous yellow chiral COF-300 membrane was fabricated. The membrane was repeatedly washed with anhydrous ethanol, 1,4-dioxane, and tetrahydrofuran. It was subsequently immersed overnight in anhydrous tetrahydrofuran and vacuum-dried at 100 °C for 12 h, resulting in the final chiral COF-300 membrane (Λ-/Δ-CCOF-300 membrane).

XRD analysis confirms that the diffraction peaks of the CCOF-300 membrane are consistent with those of COF-300 powder and align well with the simulated pattern, validating the effectiveness of this membrane fabrication method (Fig. 2b). SEM images showed that a continuous and dense CCOF-300 membrane, with a thickness of 790 nm, formed on the substrate surface (Fig. 2c–e). Additionally, the pore size distribution of the CCOF-300 membrane was analyzed, showing a uniform structure with an average pore diameter of 1.8 nm. Such well-ordered channels play a critical role in ensuring high selectivity and efficiency in chiral separation (Supplementary Fig. 13). To further assess the structural stability of the CCOF-300 membrane, we conducted an experiment where the membrane was immersed in different solvents (ethanol, methanol, and *n*-hexane) for one week. Both XRD and FT-IR analyses were performed on the membranes after immersion. The XRD analysis showed no significant changes in the diffraction patterns, indicating that the CCOF-300 membrane maintains its structural integrity across various solvents (Supplementary Fig. 14). Similarly, the FT-IR spectra revealed no noticeable differences compared to the original CCOF-300 membrane, further confirming the stability of the membrane under prolonged solvent exposure (Supplementary Fig. 15). This result highlights the robustness of the CCOF-300 membrane under different solvent conditions, which is essential for practical applications. Supplementary Fig. 16 presents the typical CD and UV–Vis absorption spectra of the CCOF-300 membranes. The CCOF-300 membranes exhibited CD signals, which are near-mirror images of each other. Λ-CCOF-300 membrane displayed a positive cotton effect at 493 nm and negative cotton effects at 332 nm, 458 nm and 548 nm, while Δ-CCOF-300 membrane exhibited a negative cotton effect at 501 nm and positive cotton effects at 327 nm, 463 nm and 556 nm. The Λ- and Δ-CCOF-300 membranes, having nearly opposite absolute configurations to each other showed opposite cotton effect signs. Although CD signals did not represent a perfect mirror correlation, this result confirmed that the preparation of chiral membranes with opposite chirality were achievable through chiral induction synthesis strategies.

In a control experiment, we introduced a chiral tartaric acid solution into the precursor solution of COF-300 and employed a polyaniline-coated aluminum oxide substrate to induce the chiral growth of COF-300 membranes. However, we were unable to fabricate continuous and dense membrane. In contrast to the synthesis method reported by Sun et al., we utilized the advantage of allowing the basic polyaniline to adsorb a substantial amount of chiral tartaric acid. The polyaniline-coated alumina substrate was modified with chiral tartaric acid, which induced the in-situ growth of the chiral COF-300 membrane. This process concentrates the chiral induction environment in the initial layer. resulting in pore channels within the subsequently grown framework that exhibit chirality, similar to the sergeants-and-soldiers effect. The sergeants-and-soldiers effect describes a phenomenon where chiral information is transmitted and amplified among molecules. It was first observed in the 1960s and was later named and described by M. Green in the context of poly(isocyanate)[75]. In this process, a small number of chiral molecules (the sergeants) direct a large number of achiral molecules (the soldiers) to form an assembly with enhanced chiral signals. In this study, the modification of polyaniline-coated aluminum oxide substrate with chiral tartaric acid results in the creation of a chiral substrate surface. Acting as a sergeant, the chiral substrate promotes the stacking of monomers in a chiral configuration. The initial layer of chiral CCOF-300 formed by the monomers acts as soldiers, aligning themselves according to the chiral surface while transmitting chiral information. The π-π stacking interactions ensure the reliable transmission of chiral configurational information along the pore walls during crystal growth, allowing the entire framework to acquire chirality through chiral induction. Ultimately, a chiral CCOF-300 membrane is fabricated.

To confirm that the chirality of the Λ-/Δ-CCOF-300 membrane arises from the overall chiral structure formed during self-assembly, FT-IR and CD measurements were performed. Initially, CD testing was conducted on a polyaniline-coated aluminum oxide substrate (PANI-Al_2O_3). Then, FT-IR and CD testing was conducted on PANI-Al_2O_3. As illustrated in Supplementary Fig. 17, FT-IR spectra show peaks at 1167 cm^{-1} (C – H), 1305 cm^{-1} (C – N), 1503 cm^{-1}, and 1593 cm^{-1} (C = C), confirming the modification of polyaniline on the aluminum oxide substrate surface. Furthermore, no CD signal was detected in the 300 – 600 nm range (Fig. 2f). After immersing PANI-Al_2O_3 in 2.0 mol L^{-1} L-tartaric acid solution (LT-PANI-Al_2O_3), FT-IR analysis revealed a peak at 1717 cm^{-1} corresponding to the carboxyl group of L-tartaric acid. CD testing revealed a signal at 220 nm, corresponding to the characteristic signal of L-tartaric acid, but no additional CD signals were observed in the 300 – 600 nm range. Subsequently, LT-PANI-Al_2O_3 was immersed separately in solutions of TAPM for 24 h. The FT-IR spectra exhibited peaks associated with the amine group of TAPM. No CD signal was detected in the 300 – 600 nm range, suggesting that chirality was not effectively transferred to the monomers before the formation of the COF lattice. In contrast, after the self-assembly of the Λ-CCOF-300 membrane, a distinct CD signal was observed in the 300 – 600 nm range. This observation is attributed to the immobilization of dihedral angles following lattice formation, resulting in the lattice achieving a stable state that typically corresponds to the system's energy minimum. In this lowest energy state, chirality is transferred and maintained.

Next, we utilized the fabricated chiral membrane for the enantioselective separation of chiral drug. Fmoc-Lys(Dde)-OH (18.8 Å × 14.6 Å × 10.1 Å), which has a molecular size compatible with the chiral pore size of CCOF-300 (ca. 18.0 Å), was selected as the target for chiral separation. Fmoc-Lys(Dde)-OH is a commonly used protecting amino acid in peptide synthesis, and it holds significant pharmaceutical value due to its pivotal role in drug development, particularly in the design of targeted therapeutics and bioactive peptides. The chiral separation performance was evaluated using a custom-designed side-by-side diffusion cell (Supplementary Fig. 30). For instance, Λ-CCOF-300 membrane was placed between two chambers, with rubber gaskets ensuring a secure seal. Both the feed and permeate sides were continuously stirred using magnetic stirrers. A 5.0 mmol L^{-1} solution of racemic Fmoc-Lys(Dde)-OH in ethanol was introduced to the feed side, while pure ethanol was used on the permeate side, with the separation process driven by a concentration gradient. Figure 3a–c show the high-performance liquid chromatography (HPLC) results from the permeate side after one hour. At this time, only Fmoc-L-Lys(Dde)-OH was detected on the permeate side, achieving the highest enantiomeric selectivity with an *ee* value of 100%. As the permeation time increased, Fmoc-D-Lys(Dde)-OH began to permeate after approximately 9 h, with the *ee* maintained at 79%. Notably, after 3 h, the flux of Fmoc-L-Lys(Dde)-OH decreased significantly, likely due to the obstruction of molecule passage by Fmoc-L-Lys(Dde)-OH accumulated within the pores (Fig. 4a). These separation experiments demonstrate the ability of the CCOF-300 membrane to effectively separate racemic mixtures of chiral compounds.

https://doi.org/10.1038/s41467-025-60572-0

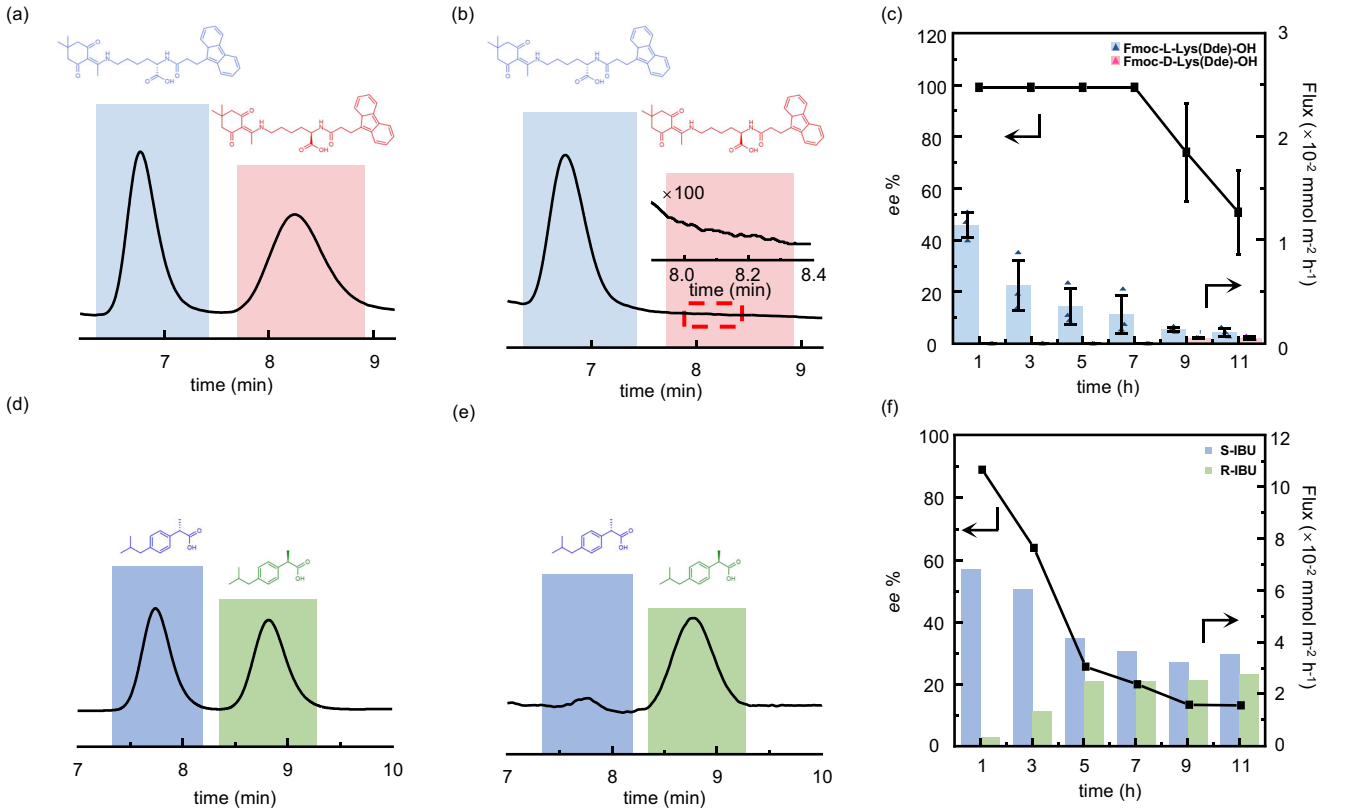

Fig. 3 | Chiral separation experiment and *ee* value of Fmoc-Lys(Dde)-OH and IBU. a HPLC result of racemic Fmoc-Lys(Dde)-OH. Retention time: Fmoc-L-Lys(Dde)-OH (light blue shadow, 6.70 min) and Fmoc-D-Lys(Dde)-OH (pink shadow, 8.17 min). **b** HPLC result of resolved Fmoc-Lys(Dde)-OH enantiomers after separation for one hour under condition of 5.0 mmol L^{-1} racemic Fmoc-Lys(Dde)-OH as feed solution at room temperature, the *ee* is 100% (Illustration shows the enlarged region of the HPLC chromatogram, × 100). **c** *ee* value of Λ-CCOF-300 membrane under condition of 5.0 mmol L^{-1} Fmoc-Lys(Dde)-OH-ethanol as feed solution at room temperature. Data are presented as mean ± standard error (SE, $n = 3$). **d** HPLC result of racemic IBU. Retention time: S-IBU (dark blue shadow, 7.85 min) and R-IBU (green shadow, 8.82 min). **e** HPLC result of resolved IBU enantiomers after separation for one hour under condition of 5.0 mmol L^{-1} racemic IBU as feed solution at room temperature, the *ee* is 88%. **f** *ee* value of Λ-CCOF-300 membrane under condition of 5.0 mmol L^{-1} IBU-ethanol as feed solution at room temperature.

In a control experiment, we employed a chiral tartaric acid-polyaniline-alumina substrate to achieve the chiral resolution of Fmoc-Lys(Dde)-OH. HPLC analysis indicated an *ee* of merely 0.36%, thereby confirming that the chiral resolution capability is derived from the chiral environment provided by the pores of the CCOF-300 membrane. The separation experiments demonstrated that the CCOF-300 membrane effectively separates racemic drug.

To investigate the effect of pore size, we selected ibuprofen (IBU, 12.9 Å × 7.0 Å × 5.5 Å), which has a molecular size smaller than the pore size of CCOF-300, as the target for chiral separation. The same chiral separation procedure was applied to racemic IBU. Figure 3d–f show the HPLC results from the permeate side after 1 h. Within the first hour, the S-IBU enantiomer was enriched over the R-IBU enantiomer, exhibiting the highest enantioselectivity with an *ee* of 88%. In contrast to the chiral separation of Fmoc-Lys(Dde)-OH, where *ee* values of 100% were maintained within a specific timeframe, the chiral separation of IBU showed the presence of both S-IBU and R-IBU enantiomers within the first hour. This disparity is likely due to the significantly smaller molecular size of IBU relative to the CCOF-300 pore size, which resulted in a lower separation efficiency and further corroborates the impact of the pore size effect on chiral resolution. Fmoc-Lys(Dde)-OH exhibits superior compatibility with the pore size of CCOF-300, resulting in enhanced separation efficiency for Fmoc-Lys(Dde)-OH. While significant advancements have been made in the separation technology for smaller chiral drug molecules[22–29], the chiral separation of larger drug molecules remains a considerable challenge. Our developed technology shows promise for the separation of large chiral drugs.

To elucidate the factors influencing the chiral separation capability of CCOF-300 membranes, we examined the underlying mechanism. Initially, we explored the interaction between the pores (binding sites) of CCOF-300 (host) and the chiral drug molecules (guest). Table 1 presents the binding affinities of CCOF-300 with various chiral drug molecules across different solvents (Details of the experimental procedures can be found in the Supplementary Information). The solvent effect on the binding affinity between chiral drug molecules and the host framework was analyzed using three solvents with distinct polarities: *n*-hexane (polarity 0.06), ethanol (polarity 4.3) and methanol (polarity 6.6). As illustrated in Table 1, the formation of the host-guest complex with Λ-CCOF-300 as the host and S-IBU as the guest showed a decrease in the binding constant (K_f) from 1.7×10^3 M^{-1} in *n*-hexane to 1.3×10^3 M^{-1} in ethanol, and further to 1.2×10^3 M^{-1} in methanol. The corresponding binding free energies ($\Delta_r G_m(T)$) were −18.4, −17.8, and −17.6 kJ mol^{-1}, respectively (Supplementary Figs. 18–23). Although differences in binding energies are present, they are negligible, suggesting that solvent polarity has minimal impact on the interaction between the chiral framework and guest drug molecules.

In our study of the chiral drug IBU and Fmoc-Lys(Dde)-OH, we observed that although these chiral drugs exhibit distinct molecular sizes, they possess a similar suite of functional groups, including carboxyl, carbonyl, and phenyl groups. These functional groups interact with the benzene rings and Schiff base groups within the CCOF-300 pore network primarily through relatively weak van der Waals forces and hydrogen bonding. Moreover, our experimental results indicate

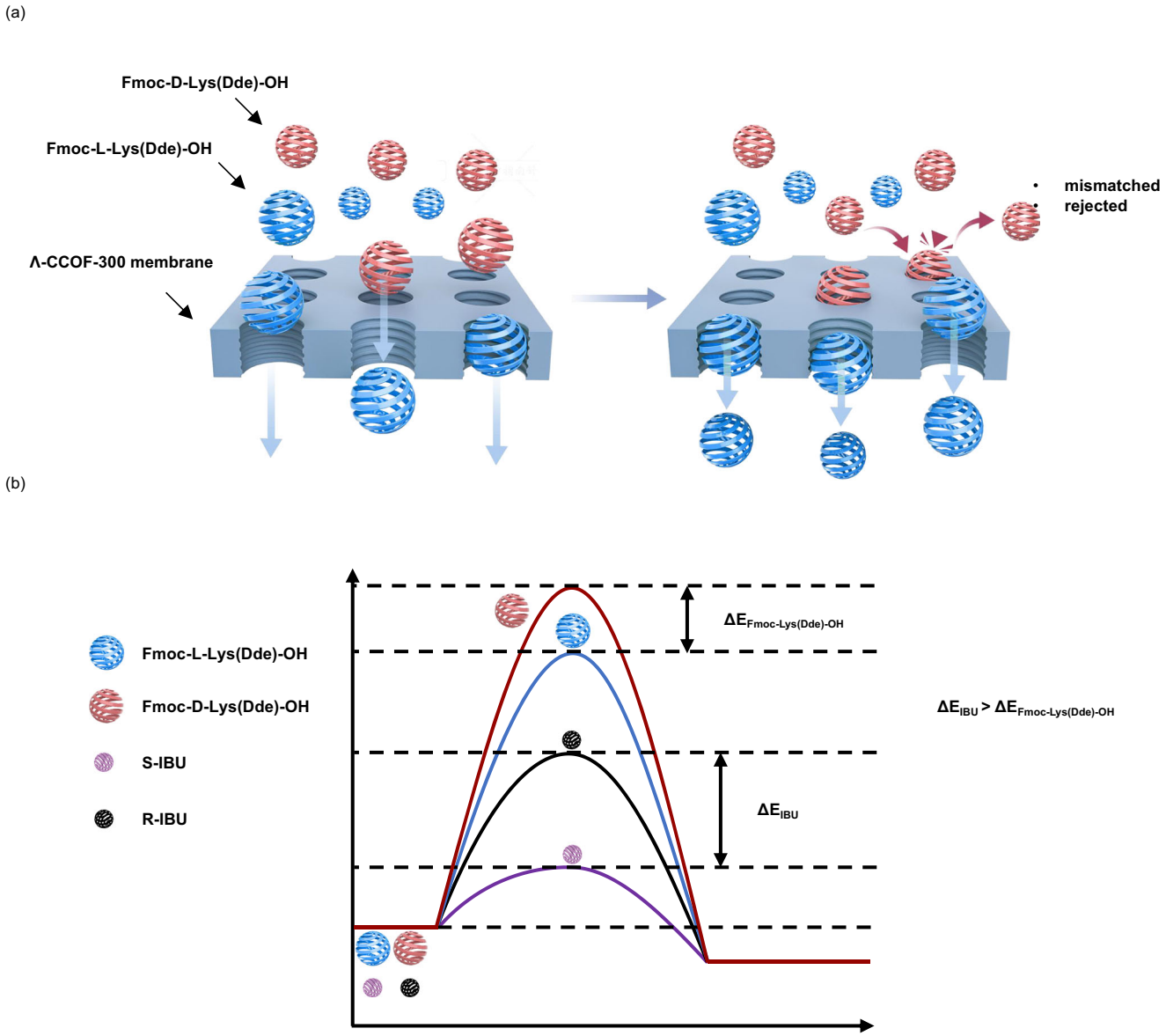

Fig. 4 | Chiral competitive diffusion and energy barriers in enantiomer separation channels. a Chiral separation channels originated from chiral competitive diffusion between two enantiomers. **b** Energy barrier required for different enantiomers to traverse chiral channels.

that the binding energy differences between chiral drug molecules and CCOF-300 are minimal, confirming that binding energy variations are not the key determinant in chiral separation.

Subsequently, the binding affinities between Fmoc-L-Lys(Dde)-OH/Fmoc-D-Lys (Dde)-OH and Λ-CCOF-300/Δ-CCOF-300 were further investigated. As illustrated in Table 1, the formation of the host-guest complex with Λ-CCOF-300 as the host and Fmoc-L-Lys(Dde)-OH as the guest showed a K_f decreasing from $2.5 \times 10^3\ M^{-1}$ in ethanol to $1.5 \times 10^3\ M^{-1}$ in methanol, with $\Delta_r G_m(T)$ of −19.4 and −18.1 kJ mol^{-1}, respectively. In contrast, for the host-guest complex with Δ-CCOF-300 as the host and Fmoc-L-Lys(Dde)-OH as the guest, the K_f decreased from $3.1 \times 10^3\ M^{-1}$ in ethanol to $1.7 \times 10^3\ M^{-1}$ in methanol, with $\Delta_r G_m(T)$ of −19.9 and −18.4 kJ mol^{-1}, respectively. The values for K_f and $\Delta_r G_m(T)$ were not provided for Fmoc-L-Lys(Dde)-OH in *n*-hexane due to its insolubility (Supplementary Figs. 24–29). Despite the differences in binding affinities between Λ-CCOF-300/Δ-CCOF-300 and Fmoc-L-Lys(Dde)-OH, the observed variations were relatively minor. Compared to the small-molecule drug IBU, the binding energy of the macromolecular drug Fmoc-L-Lys(Dde)-OH shows only a marginal increase, with a difference of just 1.6 kJ mol^{-1} in ethanol as the solvent. This indicates that the chiral channel demonstrates similar binding efficiency for both drug molecules, suggesting that binding strength is not the key determinant for enantioselective separation.

We further investigated the role of kinetics in the separation process, as detailed in the Methods section. The calculations presented in Supplementary Table 2 indicate that the diffusion rate of S-IBU through the membrane is significantly faster than that of R-IBU, with S-IBU diffusing 400 times more rapidly within the first hour. Additionally, we analyzed the diffusion rates of Fmoc-Lys(Dde)-OH enantiomers, as shown in Supplementary Table 3. The diffusion rate of Fmoc-L-Lys(Dde)-OH was 13 times greater than that of Fmoc-D-Lys(Dde)-OH within the same time frame. Compared to the smaller IBU molecules, Fmoc-L-Lys(Dde)-OH and Fmoc-D-Lys(Dde)-OH, which are compatible with the pore size of Λ-CCOF-300, exhibited a slower initial diffusion rate due to pore size effects. Supplementary Tables 2, 3 demonstrates that the diffusion barriers for the two enantiomers of IBU are lower than those for Fmoc-L-Lys(Dde)-OH. Furthermore, the more pronounced difference in diffusion rates for IBU, compared to Fmoc-Lys(Dde)-OH, indicates that the difference in diffusion barriers (ΔE) is greater than that for Fmoc-Lys(Dde)-OH (Fig. 4b).

Table 1 | Binding of CCOF-300 with chiral drugs in various solvents

Host	Guest	*n*-hexane		Ethanol		Methanol	
		K_f / M^{-1} (×10^3)	$\Delta_rG_m(T)$ / kJ mol^{-1}	K_f / M^{-1} (×10^3)	$\Delta_rG_m(T)$ / kJ mol^{-1}	K_f / M^{-1} (×10^3)	$\Delta_rG_m(T)$ / kJ mol^{-1}
Λ-CCOF-300	S-IBU	1.7	−18.4	1.3	−17.8	1.2	−17.6
	R-IBU	2.0	−18.8	1.7	−18.4	1.4	−18.0
Δ-CCOF-300	S-IBU	1.7	−18.4	1.6	−18.3	1.3	−17.8
	R-IBU	1.7	−18.4	1.4	−17.8	1.1	−17.4
Λ-CCOF-300	Fmoc-L-Lys(Dde)-OH			2.5	−19.4	1.5	−18.1
	Fmoc-D-Lys(Dde)-OH			3.2	−20.0	1.7	−18.4
Δ-CCOF-300	Fmoc-L-Lys(Dde)-OH			3.1	−19.9	1.7	−18.4
	Fmoc-D-Lys(Dde)-OH			2.6	−19.5	1.5	−18.1

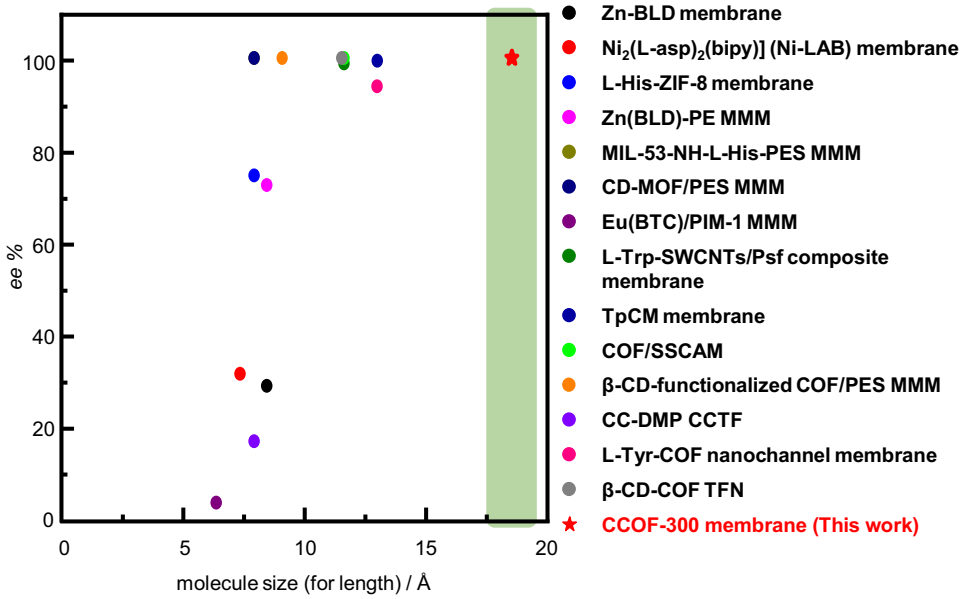

Fig. 5 | Comparative analysis of chiral separation performance. Comparison of chiral separation performance of CCOF-300 membrane with reported representative state-of-the-art enantioselective membranes[66–69,76–86].

The observed differences in the diffusion rates of IBU and Fmoc-Lys(Dde)-OH enantiomers can be attributed to the presence of chiral diffusion barriers, which result in slower diffusion rates for R-IBU and Fmoc-D-Lys(Dde)-OH compared to their respective enantiomers. The greater disparity in diffusion rates between S-IBU and R-IBU, as opposed to Fmoc-L-Lys(Dde)-OH and Fmoc-D-Lys(Dde)-OH, is due to the rigid structure of IBU, particularly in the region containing the chiral carbon. Unlike the more flexible structure of Fmoc-Lys(Dde)-OH, IBU enantiomers exhibits a higher chiral diffusion barrier difference, leading to a more pronounced difference in diffusion rates. Thus, it is concluded that the primary factor influencing the chiral separation capability of the Λ-CCOF-300 membrane is the variation in diffusion rates of the chiral drugs.

The diffusion rate of R-IBU is significantly higher than that of Fmoc-L-Lys(Dde)-OH due to the pore size effect, despite the relatively low diffusion rate of R-IBU (0.01 mmol m^{-2} h^{-1}). Consequently, absolute separation was not achieved during the chiral resolution of IBU. In contrast, absolute resolution was observed in the separation of chiral Fmoc-Lys(Dde)-OH. We conclude that absolute chiral resolution can only occur when the size of the chiral drug matches the pore size of the CCOF-300 membrane, resulting in an extremely slow diffusion rate, and when a chiral diffusion barrier exists.

To highlight the significance of our study, we compared the chiral separation performance of CCOF-300 membrane with other reported membranes, and the results are shown in Fig. 5 and Supplementary Table 4. The CCOF-300 membrane is superior to other membranes in separating large chiral drug. Unlike many existing membranes that can only separate small chiral drugs, the CCOF-300 membrane achieves 100% *ee* value when separating large chiral drug such as Fmoc-Lys(Dde)-OH. Therefore, the CCOF-300 membrane represents an important progress in the field of chiral separation, providing a highly selective and efficient separation solution for large chiral drug.

Discussion

In summary, we synthesized CCOF-300 membrane using chiral induction strategy. The membrane was prepared by embedding L-(+)-/ D-(−)-tartaric acid as a chiral dopant into a polyaniline coating on an aluminum oxide substrate, thereby achieving the preparation of the chiral-induced COF-300 membrane. The prepared CCOF-300 membrane exhibited chiral separation performance in separating the racemic Fmoc-Lys-(Dde)-OH, achieving 100% *ee*. The high separation efficiency was primarily attributed to chiral-matching diffusion (differences in diffusion rates between enantiomers) and the size matching between the chiral drugs and the membrane pore. Notably, our study further demonstrates that binding energy between the membrane and chiral drugs does not play a significant role in chiral separation. This study makes progress in the synthesis and

application of chiral separation membranes. It not only proposes a cost-effective method for chiral drug separation but also indicates the effectiveness of the chiral induction strategy in improving separation efficiency. Furthermore, it provides ideas and methods for solving the chiral separation challenges faced by the pharmaceutical industry.

Methods

Materials

Terephthalaldehyde was purchased from Tokyo Chemical industry Co. Ltd., Tetra(4-nitrophenyl)methane was purchased from Jilin Chinese Academy of Sciences-Yanshen Technology Co., Ltd., Raney-Nickel (50 μm) were purchased from Aladdin, Polyaniline (PANI) were purchased from Aladdin, *n*-hexane (≥97.0%), Methanol (≥99.5%), Ethanol (≥99.5%), CH_3COOH (≥99.5%), $N_2H_4{\cdot}H_2O$ (≥85.0%), Tetrahydrofuran (≥99.0%) were purchased from Sinopharm chemical reagent Co., Ltd., the solvents were purified and dried according to the standard techniques: 1,4-Dioxane was distilled from CaH_2. All the glass instruments were purchased from Synthware Glass. Aluminum oxide (99.99%, metals basis, Crystal form α, 0.20 μm) were purchased from Aladdin. Emery paper (800 mesh and 2000 mesh) was purchased from Shanghai New Five Kyrgyzstant Abrasives Co. Ltd., Teflon reactors were purchased from Jinan Henghua Sci.

Instrumentation

^{1}H NMR spectra were measured on a Bruker Fourier 600 MHz spectrometer. Unless otherwise stated, all spectra were measured at ambient temperature. The FT-IR spectra (KBr) were obtained using a SHIMADZU IRAffinity−1 Fourier transform infrared spectrophotometer. A SHIMADZU UV-2450 spectrophotometer was used for all absorbance measurements. XRD measurements were carried out using Bruker D8 Advance X-ray diffractometer with Cu-Kα radiation, 40 kV, 40 mA and scanning rate of 0.30 min^{-1} (2θ). The powdered sample was added to the glass and compacted for measurement. SEM and elemental mapping analysis were carried out with ZEISS Gemini-SEM. VCD spectra were obtained using ChiralIR-2X. The CD spectra were obtained using JASCO J-1500.

Synthesis of TAPM

Hydrazine hydrate (4.0 g, 79.9 mmol) was added dropwise to a suspension of Raney Ni (20.0 g) and tetra(4-nitrophenyl)methane (3.0 g, 6.0 mmol) in tetrahydrofuran (200 mL). After heating at 75 °C for 4 h, the mixture was filtered while still hot. The filtrate was then concentrated by rotary evaporation to remove the solvent, yielding a white solid of TAPM (2.4 g, 80%).

Preparation of CCOF-300 membranes

Porous alumina sheets were selected as substrates and modified them with polyaniline via spin coating, followed by immersion in a 2.0 mol L^{-1} solution of L-(+)- or D-(−)-tartaric acid for secondary modification. The color of the polyaniline-coated aluminum oxide substrates transitioned from blue to green during this period. The specific preparation steps of CCOF-300 membrane are as follows: 36.0 mg (0.3 mmol) of TPA and 60.0 mg (0.2 mmol) of TAPM were added to the 50 mL reactor. Subsequently, 9 mL of anhydrous 1, 4-dioxane was added and ultrasonically mixed to thoroughly dissolve the aforementioned raw materials. This process yielded a clear yellow solution. We then gradually added 0.6 mL of 3 M acetic acid aqueous solution to the solution while stirring. Following completion of the preceding processes, the modified substrate was quickly placed into the reactor, making sure that the modified side was facing up, and then the reactor was sealed. After 24 h of processing at 100 °C, a continuous yellow CCOF-300 membrane was fabricated. The CCOF-300 membrane was sequentially cleaned with anhydrous ethanol, 1,4-dioxane, and tetrahydrofuran. It was then immersed in fresh tetrahydrofuran, with solvent changes every 4 h, followed by an overnight immersion to remove residual impurities. Finally, the membrane was vacuum-dried at 100 °C for 12 h.

Chiral separation experiment

Two chambers were connected with clamp serve as the dialyzers. Λ-CCOF-300 membrane was placed between the two chambers and the rubber gaskets were used to seal the connection. The feed side and the permeate side were continuously stirred by magnetic stirring apparatus. Racemic Fmoc-Lys(Dde)-OH or IBU dissolved in ethanol, with a concentration of 5.0 mmol L^{-1}, were introduced to the feed side, while the pure ethanol solvent was used at the permeate side.

The enantiomeric concentration was analyzed with a HPLC system. Chromatographic separations were performed at 40 °C using a CHIRALPAK AD-RH column (5 μm, 4.6 mm × 150 mm). The analyses of Fmoc-Lys(Dde)-OH were performed by a UV detector at 263 nm using a mobile phase consisting of 80% acetonitrile, 20% phosphoric acid aqueous solution at a flow rate of 0.4 mL min^{-1}. The injected sample volume was 10 μL (The analyses of IBU were performed by a UV detector at 254 nm using a mobile phase consisting of 70% methanol, 30% phosphoric acid aqueous solution at a flow rate of 0.7 mL min^{-1}. The injected sample volume was 10 μL.).

The *ee* was determined from the peak areas of their two enantiomers, S-isomer (A_S) and R-isomer (A_R).

$$ee\,\% = 100 \times \frac{\left|A_R - A_S\right|}{A_S + A_R} \tag{1}$$

Permeation flux test

For the determination of permeation flux, Fmoc-L-Lys(Dde)-OH or Fmoc-D-Lys(Dde)-OH (S-IBU or R-IBU) ethanol solution was introduced into the feed side, and pure ethanol was introduced into the permeation side. Hourly samples were collected, and the single-enantiomer concentration in the permeation side was analyzed using HPLC to determine the penetration flux.

The permeation flux of the CCOF-300 membrane can be written as:

$$\text{Flux} = \frac{n}{A \times t} \tag{2}$$

where n is the permeated R- or S- enantiomer (L- or D- enantiomer) (mol), A and t refer to the effective membrane area (m^2) and the permeation time (h), respectively.

Data availability

The data that support the findings detailed in this study are available within the article and supplementary information as well as on figshare https://doi.org/10.6084/m9.figshare.29115320. All data are available from the corresponding author upon request.

References

1. Pinto, M. M., Fernandes, C. & Tiritan, M. E. Chiral separations in preparative scale: a medicinal chemistry point of view. *Molecules* **25**, 1931 (2020).
2. Vedovello, P., Paranhos, C. M., Fernandes, C. & Tiritan, M. E. Chiral polymeric membranes: Recent applications and trends. *Sep. Purif. Technol.* **280**, 119800 (2022).
3. Kandula, J. S., Rayala, V. P. K. & Pullapanthula, R. Chirality: an inescapable concept for the pharmaceutical, bio-pharmaceutical, food, and cosmetic industries. *Sep Sci.* **6**, 2200131 (2023).
4. Hancu, G. & Modroiu, A. Chiral switch: Between therapeutical benefit and marketing strategy. *Pharmaceuticals* **15**, 240 (2022).

5. Evans, A. M. Comparative pharmacology of S (+)-ibuprofen and (RS)-ibuprofen. *Clin. Rheumatol.* **20**, 9–14 (2001).
6. Hutt, A. J. The development of single-isomer molecules: why and how. *CNS Spectr.* **7**, 14–22 (2002).
7. Hutt, A. J. Chirality and pharmacokinetics: an area of neglected dimensionality?. *drug Metab. drug Interact.* **22**, 79–112 (2007).
8. Jemec, G. et al. A randomized controlled trial of R-salbutamol for topical treatment of discoid lupus erythematosus. *Br. J. Dermatol* **161**, 1365–1370 (2009).
9. Punj, A., Prakash, A. & Bhasin, A. Levosalbutamol vs racemic salbutamol in the treatment of acute exacerbation of asthma. *Indian J. Pediatr.* **76**, 1131–1135 (2009).
10. Daniel, K. G., Guida, W. C. & Brooks, W. H. The Significance of Chirality in Drug Design and Development. *Curr. Top. Med. Chem.* **11**, 760–770 (2011).
11. Sekhon, B. S. Exploiting the power of stereochemistry in drugs: an overview of racemic and enantiopure drugs. *J. Mod. Med. Chem.* **1**, 10–36 (2013).
12. Ide, S. & Ikeda, K. Mechanisms of the antidepressant effects of ketamine enantiomers and their metabolites. *Biol. Psychiatry* **84**, 551–552 (2018).
13. Ribeiro, C. et al. Chiral drug analysis in forensic chemistry: an overview. *Molecules* **23**, 262 (2018).
14. Bitchagno, G. T. M., Nchiozem-Ngnitedem, V.-A., Melchert, D. & Fobofou, S. A. Demystifying racemic natural products in the homochiral world. *Nat. Chem. Rev.* **6**, 806–822 (2022).
15. Jung, W., Kwon, J., Cho, W. & Yeom, J. Chiral biomaterials for nanomedicines: From molecules to supraparticles. *Pharmaceutics* **14**, 1951 (2022).
16. Ceramella, J. et al. A look at the importance of chirality in drug activity: Some significative examples. *Appl. Sci.* **12**, 10909 (2022).
17. Johnston, J. N., Henter, I. D. & Zarate, C. A. Jr The antidepressant actions of ketamine and its enantiomers. *Pharm. Ther.* **246**, 108431 (2023).
18. Sanganyado, E., Lu, Z., Fu, Q., Schlenk, D. & Gan, J. Chiral pharmaceuticals: A review on their environmental occurrence and fate processes. *Water Res.* **124**, 527–542 (2017).
19. Zhou, Y. et al. Chiral pharmaceuticals: environment sources, potential human health impacts, remediation technologies and future perspective. *Environ. Int.* **121**, 523–537 (2018).
20. Sui, J. et al. Strategies for chiral separation: from racemate to enantiomer. *Chem. Sci.* **14**, 11955–12003 (2023).
21. Zhu, Q., Cai, Z., Zhou, P., Sun, X. & Xu, J. Recent progress of membrane technology for chiral separation: a comprehensive review. *Sep. Purif. Technol.* **309**, 123077 (2023).
22. Woiwode, U., Neubauer, S., Lindner, W., Buckenmaier, S. & Lämmerhofer, M. Enantioselective multiple heartcut two-dimensional ultra-high-performance liquid chromatography method with a Coreshell chiral stationary phase in the second dimension for analysis of all proteinogenic amino acids in a single run. *J. Chromatogr. A* **1562**, 69–77 (2018).
23. Felletti, S. et al. Recent achievements and future challenges in supercritical fluid chromatography for the enantioselective separation of chiral pharmaceuticals. *Chromatographia* **82**, 65–75 (2019).
24. Folprechtová, D. et al. Enantioseparation performance of superficially porous particle vancomycin-based chiral stationary phases in supercritical fluid chromatography and high performance liquid chromatography; applicability for psychoactive substances. *J. Chromatogr. A* **1637**, 461846 (2021).
25. Fanali, S. & Chankvetadze, B. History, advancement, bottlenecks, and future of chiral capillary electrochromatography. *J. Chromatogr. A* **1637**, 461832 (2021).
26. Betzenbichler, G. et al. Chiral stationary phases and applications in gas chromatography. *Chirality* **34**, 732–759 (2022).
27. Putman, J. I. & Armstrong, D. W. Recent advances in the field of chiral crystallization. *Chirality* **34**, 1338–1354 (2022).
28. de Jesús Cruz, P., Cassels, W. R., Chen, C.-H. & Johnson, J. S. Doubly stereoconvergent crystallization enabled by asymmetric catalysis. *Science* **376**, 1224–1230 (2022).
29. Tamatam, R. & Shin, D. Asymmetric Synthesis of US-FDA Approved Drugs over Five Years (2016–2020): A Recapitulation of Chirality. *Pharmaceuticals* **16**, 339 (2023).
30. Lemasson, E., Bertin, S. & West, C. Use and practice of achiral and chiral supercritical fluid chromatography in pharmaceutical analysis and purification. *J. Sep. Sci.* **39**, 212–233 (2016).
31. Shen, J. & Okamoto, Y. Efficient separation of enantiomers using stereoregular chiral polymers. *Chem. Rev.* **116**, 1094–1138 (2016).
32. West, C. Recent trends in chiral supercritical fluid chromatography. *TrAC Trends Anal. Chem.* **120**, 115648 (2019).
33. Al-Sulaimi, S. et al. Emerging developments in separation techniques and analysis of chiral pharmaceuticals. *Molecules* **28**, 6175 (2023).
34. Kumari Rayala, V. P., Kandula, J. S. & P, R. Advances and challenges in the pharmacokinetics and bioanalysis of chiral drugs. *Chirality* **34**, 1298–1310 (2022).
35. Seo, J. S. et al. A homochiral metal–organic porous material for enantioselective separation and catalysis. *Nature* **404**, 982–986 (2000).
36. Kepert, C., Prior, T. & Rosseinsky, M. A versatile family of interconvertible microporous chiral molecular frameworks: the first example of ligand control of network chirality. *J. Am. Chem. Soc.* **122**, 5158–5168 (2000).
37. Bradshaw, D., Prior, T. J., Cussen, E. J., Claridge, J. B. & Rosseinsky, M. J. Permanent microporosity and enantioselective sorption in a chiral open framework. *J. Am. Chem. Soc.* **126**, 6106–6114 (2004).
38. Zhang, J. et al. Manganese and magnesium homochiral materials: decoration of honeycomb channels with homochiral chains. *J. Am. Chem. Soc.* **129**, 14168–14169 (2007).
39. Ma, L., Abney, C. & Lin, W. Enantioselective catalysis with homochiral metal–organic frameworks. *Chem. Soc. Rev.* **38**, 1248–1256 (2009).
40. Chen, S., Zhang, J., Wu, T., Feng, P. & Bu, X. Multiroute synthesis of porous anionic frameworks and size-tunable extraframework organic cation-controlled gas sorption properties. *J. Am. Chem. Soc.* **131**, 16027–16029 (2009).
41. Zhang, J. et al. A tale of three carboxylates: Cooperative asymmetric crystallization of three-dimensional microporous framework from achiral precursors. *Angew. Chem. Int. Ed.* **49**, 1267–1270 (2010).
42. Liu, Y., Xuan, W. & Cui, Y. Engineering homochiral metal-organic frameworks for heterogeneous asymmetric catalysis and enantioselective separation. *Adv. Mater.* **22**, 4112–4135 (2010).
43. Corella-Ochoa, M. N. et al. Homochiral metal–organic frameworks for enantioselective separations in liquid chromatography. *J. Am. Chem. Soc.* **141**, 14306–14316 (2019).
44. Han, Z. et al. Cation-induced chirality in a bifunctional metal-organic framework for quantitative enantioselective recognition. *Nat. Commun.* **10**, 5117 (2019).
45. Chen, T., Li, H., Shi, X., Imbrogno, J. & Zhao, D. Robust Homochiral Polycrystalline Metal–Organic Framework Membranes for High-Performance Enantioselective Separation. *J. Am. Chem. Soc.* **146**, 14433–14438 (2024).
46. Wang, X. et al. Homochiral 2D Porous Covalent Organic Frameworks for Heterogeneous Asymmetric Catalysis. *J. Am. Chem. Soc.* **138**, 12332–12335 (2016).
47. Wang, L. K. et al. Divergent synthesis of chiral covalent organic frameworks. *Angew. Chem. Int. Ed.* **131**, 9543–9547 (2019).
48. Yuan, C. et al. Crystalline C—C and C═ C bond-linked chiral covalent organic frameworks. *J. Am. Chem. Soc.* **143**, 369–381 (2020).

49. Chen, M., Zhang, J., Liu, C., Li, H. & Zhang, B. Construction of Pyridine-Based Chiral Ionic Covalent Organic Frameworks as a Heterogeneous Catalyst for Promoting Asymmetric Henry Reactions. *Org. Lett.* **23**, 1748–1752 (2021).
50. Tang, X. et al. Self-Assembly of Helical Nanofibrous Chiral Covalent Organic Frameworks. *Angew. Chem. Int. Ed.* **62**, e202216310 (2023).
51. Yin, Z. et al. Metal-Free Heterogeneous Asymmetric Hydrogenation of Olefins Promoted by Chiral Frustrated Lewis Pair Framework. *J. Am. Chem. Soc.* **146**, 979–987 (2023).
52. Ma, M. et al. A review on chiral metal–organic frameworks: synthesis and asymmetric applications. *Nanoscale* **14**, 13405–13427 (2022).
53. Yoon, M., Srirambalaji, R. & Kim, K. Homochiral metal–organic frameworks for asymmetric heterogeneous catalysis. *Chem. Rev.* **112**, 1196–1231 (2012).
54. Zhu, G. et al. Development and application of chiral separation technology based on chiral metal-organic frameworks. *J. Pharm. Anal.* 101176 https://doi.org/10.1016/j.jpha.2024.101176 (2024).
55. Han, X. et al. Chiral covalent organic frameworks: design, synthesis and property. *Chem. Soc. Rev.* **49**, 6248–6272 (2020).
56. Sun, Z., Hou, J., Li, L. & Tang, Z. Nanoporous materials for chiral resolution. *Coord. Chem. Rev.* **425**, 213481 (2020).
57. Yamamoto, T., Murakami, R., Komatsu, S. & Suginome, M. Chirality-Amplifying, Dynamic Induction of Single-Handed Helix by Chiral Guests to Macromolecular Chiral Catalysts Bearing Boronyl Pendants as Receptor Sites. *J. Am. Chem. Soc.* **140**, 3867–3870 (2018).
58. Xing, P. et al. Occurrence of Chiral Nanostructures Induced by Multiple Hydrogen Bonds. *J. Am. Chem. Soc.* **141**, 9946–9954 (2019).
59. Lin, Z., Slawin, A. M. & Morris, R. E. Chiral induction in the ionothermal synthesis of a 3-D coordination polymer. *J. Am. Chem. Soc.* **129**, 4880–4881 (2007).
60. Zhang, J., Chen, S., Wu, T., Feng, P. & Bu, X. Homochiral crystallization of microporous framework materials from achiral precursors by chiral catalysis. *J. Am. Chem. Soc.* **130**, 12882–12883 (2008).
61. Wang, J.-C., Kan, X., Shang, J.-Y., Qiao, H. & Dong, Y.-B. Catalytic asymmetric synthesis of chiral covalent organic frameworks from prochiral monomers for heterogeneous asymmetric catalysis. *J. Am. Chem. Soc.* **142**, 16915–16920 (2020).
62. Zhang, S.-Y. et al. Synthesis of a chiral crystal form of MOF-5, CMOF-5, by chiral induction. *J. Am. Chem. Soc.* **137**, 15406–15409 (2015).
63. Han, Y.-H. et al. Chiral template induced homochiral MOFs built from achiral components: SHG enhancement and enantioselective sensing of chiral alkamines by ion-exchange. *Chem. Commun.* **51**, 14481–14484 (2015).
64. Wu, D. et al. Induction of chirality in a metal–organic framework built from achiral precursors. *Angew. Chem. Int. Ed.* **133**, 3124–3131 (2021).
65. Han, X. et al. Chiral induction in covalent organic frameworks. *Nat. Commun.* **9**, 1294 (2018).
66. Das, S., Xu, S., Ben, T. & Qiu, S. Chiral Recognition and Separation by Chirality-Enriched Metal–Organic Frameworks. *Angew. Chem. Int. Ed.* **57**, 8629–8633 (2018).
67. Zhang, S., Zhou, J. & Li, H. Chiral covalent organic framework packed nanochannel membrane for enantioseparation. *Angew. Chem. Int. Ed.* **134**, e202204012 (2022).
68. Chen, W. et al. Preparation and application of a chiral Am7CD-modified COF composite membrane by interfacial polymerization. *Sep. Purif. Technol.* **323**, 124406 (2023).
69. Chen, Y., Xia, L., Lu, Z., Li, G. & Hu, Y. In situ fabrication of chiral covalent triazine frameworks membranes for enantiomer separation. *J. Chromatogr. A* **1654**, 462475 (2021).
70. Uribe-Romo, F. J. et al. A crystalline imine-linked 3-D porous covalent organic framework. *J. Am. Chem. Soc.* **131**, 4570–4571 (2009).
71. Zhou, Z. et al. Conformational Chirality of Single-Crystal Covalent Organic Frameworks. *J. Am. Chem. Soc.* **146**, 34064–34069 (2024).
72. Fu, J. et al. Fabrication of COF-MOF composite membranes and their highly selective separation of H2/CO2. *J. Am. Chem. Soc.* **138**, 7673–7680 (2016).
73. Asturias, G. E., Jang, G. W., Macdiarmid, A. G., Doblhofer, K. & Zhong, C. Membrane-Properties of Polymer Films: The Acid-Doping Reaction of Polyaniline. *Ber. Bunsen-Ges. Phys. Chem.* **95**, 1381–1384 (1991).
74. Kolla, H. S., Surwade, S. P., Zhang, X., MacDiarmid, A. G. & Manohar, S. K. Absolute molecular weight of polyaniline. *J. Am. Chem. Soc.* **127**, 16770–16771 (2005).
75. Green, M. M. et al. A helical polymer with a cooperative response to chiral information. *Science* **268**, 1860–1866 (1995).
76. Wang, W. et al. A homochiral metal-organic framework membrane for enantioselective separation. *Chem. Commun.* **48**, 7022–7024 (2012).
77. Kang, Z. et al. Single nickel source" in situ fabrication of a stable homochiral MOF membrane with chiral resolution properties. *Chem. Commun.* **49**, 10569–10571 (2013).
78. Huang, K., Dong, X., Ren, R. & Jin, W. Fabrication of homochiral metal-organic framework membrane for enantioseparation of racemic diols. *AlChE J.* **59**, 4364–4372 (2013).
79. Chan, J. Y. et al. Incorporation of homochirality into a zeolitic imidazolate framework membrane for efficient chiral separation. *Angew. Chem. Int. Ed.* **130**, 17376–17380 (2018).
80. Wang, H. et al. Membrane adsorbers with ultrahigh metal-organic framework loading for high flux separations. *Nat. Commun.* **10**, 4204 (2019).
81. Lu, Y. et al. Homochiral MOF–polymer mixed matrix membranes for efficient separation of chiral molecules. *Angew. Chem. Int. Ed.* **131**, 17084–17091 (2019).
82. Lu, Y. et al. Cyclodextrin metal-organic framework-polymer composite membranes towards ultimate and stable enantioselectivity. *J. Membr. Sci.* **620**, 118956 (2021).
83. Gogoi, M., Goswami, R., Ingole, P. & Hazarika, S. Selective permeation of L-tyrosine through functionalized single-walled carbon nanotube thin film nanocomposite membrane. *Sep. Purif. Technol.* **233**, 116061 (2020).
84. Manoranjan, N., Fang, W., Zhu, Y. & Jin, J. A Chiral COFs Membrane for Enantioselective Amino Acid Separation. *Angew. Chem. Int. Ed.* **64**, e202417088 (2025).
85. Yuan, C. et al. Nanochannels of covalent organic frameworks for chiral selective transmembrane transport of amino acids. *J. Am. Chem. Soc.* **141**, 20187–20197 (2019).
86. Luo, H. et al. β-Cyclodextrin covalent organic framework modified-cellulose acetate membranes for enantioseparation of chiral drugs. *Sep. Purif. Technol.* **285**, 120336 (2022).

Acknowledgements

This study was supported by the National Key R&D Program of China (2021YFA1200400), the National Natural Science Foundation of China (No. 91956108, 22475194).

Author contributions

T.B. initiated and led the research project. X.G. performed the synthesis and characterization of the samples, conducted XRD, FT-IR, SEM, and CD measurements, and performed chiral separation experiment and permeation flux test. T.B. and X.G. analyzed the data and wrote the paper.

Competing interests

The authors declare no competing interests.

Additional information

Supplementary information The online version contains supplementary material available at https://doi.org/10.1038/s41467-025-60572-0.

Correspondence and requests for materials should be addressed to Teng Ben.

Peer review information *Nature Communications* thanks the anonymous, reviewer(s) for their contribution to the peer review of this work. A peer review file is available.